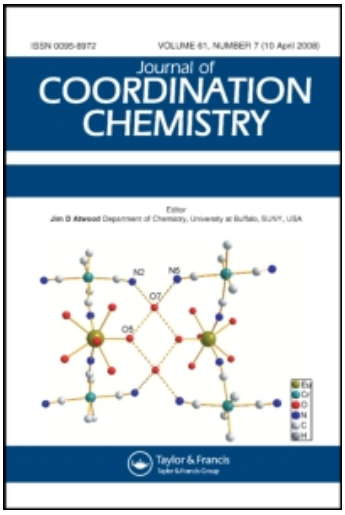

Journal of Coordination Chemistry
Publication details, including instructions for authors and subscription information:
http://www.informaworld.com/smpp/title~content=t713455674

A new pyrimidine-derived ligand, *N*-pyrimidine oxalamic acid, and its Cu(II), Co(II), Mn(II), Ni(II), Zn(II), Cd(II), and Pd(II) complexes: synthesis, characterization, electrochemical properties, and biological activity

Mehmet Sönmez[a]; Metın Çelebı[a]; Abdulkadır Levent[a]; İsmet Berber[b]; Zühre Şentürk[a]
[a] Department of Chemistry, Yüzüncü Yıl University, 65080 Van, Turkey [b] Department of Biology, Sinop University, 57000 Sinop, Turkey

Online publication date: 08 March 2010

To cite this Article Sönmez, Mehmet , Çelebı, Metın , Levent, Abdulkadır , Berber, İsmet and Şentürk, Zühre(2010) 'A new pyrimidine-derived ligand, *N*-pyrimidine oxalamic acid, and its Cu(II), Co(II), Mn(II), Ni(II), Zn(II), Cd(II), and Pd(II) complexes: synthesis, characterization, electrochemical properties, and biological activity', Journal of Coordination Chemistry, 63: 5, 848 — 860
To link to this Article: DOI: 10.1080/00958971003646506
URL: http://dx.doi.org/10.1080/00958971003646506

Journal of Coordination Chemistry
Vol. 63, No. 5, 10 March 2010, 848–860

Taylor & Francis
Taylor & Francis Group

A new pyrimidine-derived ligand, *N*-pyrimidine oxalamic acid, and its Cu(II), Co(II), Mn(II), Ni(II), Zn(II), Cd(II), and Pd(II) complexes: synthesis, characterization, electrochemical properties, and biological activity

MEHMET SÖNMEZ*†, METIN ÇELEBI†, ABDULKADIR LEVENT†, İSMET BERBER‡ and ZÜHRE ŞENTÜRK†

†Department of Chemistry, Yüzüncü Yıl University, 65080 Van, Turkey
‡Department of Biology, Sinop University, 57000 Sinop, Turkey

(*Received 19 June 2009; in final form 27 October 2009*)

A new heterocyclic compound *N*-(5-benzoyl-2-oxo-4-phenyl-2H-pyrimidin-1-yl)-oxalamic acid has been synthesized from *N*-amino pyrimidine-2-one and oxalylchloride. Bis-chelate complexes of the ligand were prepared from acetate/chloride salts of Cu(II), Co(II), Mn(II), Ni(II), Zn(II), Cd(II), and Pd(II) in methanol. The structures of the ligand and its metal complexes were characterized by microanalyses, IR, AAS, NMR, API-ES, UV-Vis spectroscopy, magnetic susceptibility, and thermogravimetric analyses. An octahedral geometry has been suggested for all the complexes, except for Pd(II) complex, in which the metal center is square planar. Each ligand binds using C(2)=O, HN, and carboxylate. The cyclic voltammograms of the ligand and the complexes are also discussed. The new synthesized compounds were evaluated for antimicrobial activities against Gram-positive, Gram-negative bacteria and fungi using the microdilution procedure. The Cu(II) complex displayed selective and effective antibacterial activity against one Gram-positive spore-forming bacterium (*Bacillus cereus* ATCC 7064), two Gram-positive bacteria (*Staphylococcus aureus* ATCC 6538 and *S. aureus* ATCC 25923) at 40–80 $\mu g\,mL^{-1}$, but poor activity against *Candida* species. The Cu(II) complex might be a new antibacterial agent against Gram-positive bacteria.

Keywords: *N*-aminopyrimidine; Metal complexes; Cyclic voltammetry; Biological activity

1. Introduction

Pyrimidine derivatives have therapeutic applications; the presence of a pyrimidine ring system in nucleic acids, vitamins, coenzymes, and antibiotics is a possible reason for their biological activity [1, 2]. Pyrimidine, as a ligand, provides potential binding sites for metal ions, and information on their coordinating properties is important to understand the role of metal ions in biological systems [3]. Considerable attention has been given to metal(II) complexes of ligands containing *N*-pyrimidine, due to their structural richness, electrochemical properties, and models for biological systems [4–7]. Purines and pyrimidines and their derivatives are growth factor analogs and have been

*Corresponding author. Email: vansonmez@hotmail.com

Journal of Coordination Chemistry
ISSN 0095-8972 print/ISSN 1029-0389 online
DOI: 10.1080/00958971003646506

used for treatment of bacterial, viral, and fungal infections [8]; pyrimidines and their complexes display effective and selective antimicrobial activity against bacteria, fungi, and viruses [9–11]. Metal(II) complexes of polydentate Schiff-base ligands of *N*-aminopyrimidines [6] acts as a bidentate or tridentate monobasic donor for Cu(II), Co(II), Ni(II), Mn(II), and Fe(III), coordinating through nitrogen of the azomethine group and oxygen of the hydroxyl group.

The goal of this study is to prepare and characterize a pyrimidine-derived ligand and its metal complexes with Cu(II), Co(II), Mn(II), Ni(II), Zn(II), Cd(II), and Pd(II). In continuation of the study, all synthesized compounds have been investigated for their electrochemical properties and antimicrobial activity.

2. Experimental

2.1. *Materials*

All chemicals used in this study were obtained commercially and used without purification. 1-Amino-5-benzoyl-4-phenyl-1*H*-pyrimidine-2-one (*N*-aminopyrimidine) was prepared according to the literature method [12].

2.2. *Physical measurements*

Elemental analyses (C, H, N, S) were performed with a Leco CHNS model 932 elemental analyzer. IR spectra were obtained using KBr pellets (4000–400 cm^{-1}) on a Bio-Rad-Win-IR spectrophotometer. Electronic spectra in the 200–900 nm range were recorded in DMF on a Unicam UV2-100 UV-Vis spectrophotometer. Magnetic measurements were carried out by the Gouy method using $Hg[Co(SCN)_4]$ as calibrant. Molar conductances of the Schiff base and metal complexes were determined in DMF at room temperature using a Jenway model 4070 conductivity meter. The ^1H- and ^{13}C-NMR spectra of the Schiff base were carried out using a Bruker 300 MHz Ultrashield TM-NMR instrument. LC/MS-API-ES mass spectra were recorded with an Agilent model 1100 MSD mass spectrophotometer. Thermogravimetric (TGA) measurements were obtained by a Shimadzu-50 thermal analyzer. The atomic absorption measurements for the determination of cobalt and nickel ion were carried out using a Thermo Solar System Atomic Absorption Spectrophotometer. For AAS, cobalt and nickel were measured using the following settings: flame type, air–acetylene; wavelength, 240.7 and 232.0 nm, respectively; lamp current, 75%; fuel flow, 0.9 L min^{-1}; burner height, 12.0 mm; band pass, 0.5 nm; measurement, 4 s. Electrochemical measurements were performed on a BAS 100 W electrochemical analyzer (Bioanalytical System, USA) using a three-electrode system, glassy carbon working electrode ($\Phi = 3$ mm, BAS), platinum wire as auxiliary electrode, and Ag/AgCl (NaCl 3M, Model RE-1, BAS, USA) as reference electrode. The reference electrode was separated from the bulk solution by a fritted-glass bridge filled with the solvent/supporting electrolyte mixture. Before each experiment, the glassy carbon electrode was polished manually with alumina ($\Phi = 0.01$ μm). Cyclic voltammetric experiments were recorded at room temperature in DMSO (in case of Pd(II) complex, in DMF) and ionic strength was maintained at 0.1 M L^{-1} with $LiClO_4$ as the supporting electrolyte.

The solutions were deoxygenated by a stream of high purity nitrogen for 15 min prior to the experiments, and during the experiments nitrogen flow was maintained over the solution.

2.3. *Synthesis of the ligand*

The ligand *N*-(5-benzoyl-2-oxo-4-phenyl-2H-pyrimidin-1-yl)-oxalamic acid (*N*-POAH) was prepared by the condensation of *N*-aminopyrimidine and oxalylchloride. *N*-aminopyrimidine (1 mM) was dissolved in hot toluene (40 mL), followed by the addition of pyridine (2 mM) to this solution. To the mixture was slowly added a solution of oxalylchloride (1 mM) in dry toluene (10 mL). A pale yellow precipitate formed at once. This resulting mixture was stirred at room temperature for 6 h and the precipitate was filtered. The solid product was warmed in water (30 mL) with stirring for 1 h, filtered, washed with water and diethyl ether, and then dried in vacuum over P_2O_5. The product was finally recrystallized from acetonitrile yielding pale yellow crystals of *N*-POAH (0.280 g, 78%); m.p.: 283°C. Anal. Calcd (%) for $C_{19}H_{13}N_3O_5$ (363):C, 62.81; H, 3.58; N, 11.57. Found: C, 63.19; H, 3.72; N, 11.58. Selected IR data (ν, cm^{-1}): 3440 (OH/NH), 1712 (COOH), 1680 (Ph-CO–), 1658 (–C=O)$_{pyrimidine}$, 1613 (NH–C=O)$_{amide}$; ^{1}H-NMR ($CDCl_3$), δ 12.4 (bs, 1H, COOH), 9.1 (s, 1H, NH), 8.7 (s, 1H, C(6)H, 6.8–7.9 (m, 10H, Harm); ^{13}C-NMR ($CDCl_3$), δ 191.3 (OC–Ar), 173.7 (−COOH), 157.7 (–CO–NH–), 153.9 (–C2, pyrimidine ring), 151.7 (–C6, pyrimidine ring), 116.8 (–C5), 128.8–137.0 (C, phenyl). UV-Vis (in DMF, nm): 202, 212, 279, 285, 343. LC-MS, *m*/*z* 362 $[M]^+$.

2.4. *Synthesis of the complexes*

$[Cu(N\text{-}POA)_2]\cdot 2H_2O$: 1 mM (0.363 g) of *N*-POAH was dissolved in chloroform and methanol mixture (50 mL; 1 : 1, v/v) and a solution of 0.5 mM (0.100 g) of $Cu(CH_3COO)_2\cdot H_2O$ in 15 mL methanol was added dropwise with continuous stirring. The mixture was stirred for 1 h at 60°C. The precipitated green compound was removed by filtration, washed with diethyl ether and cold methanol, and dried in a vacuum desiccator. Yield: 0.210 g (76%); m.p.: 248°C. Anal. Calcd (%) for $C_{38}H_{28}CuN_6O_{12}$ (823.54): C, 55.37; H, 3.40; N, 10.20; Cu, 7.72. Found: C, 55.70; H, 3.60; N, 10.40; Cu, 8.03. Selected IR data (ν, cm^{-1}): 3423 ν(NH–OH/H_2O), 1668 ν(Ph–CO), 1650 ν(C=O), 1594 ν(C=O ↔ C=N). μ_{eff}: 1.95 BM. Λ_M (10^{-3} M, in DMF, S cm^2 M^{-1}): 6.9. UV-Vis (in DMF, nm): 226, 243, 280, 323, 362, 393, 511, 697. API-ES, *m*/*z*: 701 $[(2L+Cu)-2CO_2]^+$ (^{65}Cu isotope).

The complexes $[Co(N\text{-}POA)_2]\cdot 3H_2O$, $[Ni(N\text{-}POA)_2]\cdot 2H_2O$, $[Mn(N\text{-}POA)_2]\cdot 2H_2O$, $[Zn(N\text{-}POA)_2]\cdot 2H_2O$, and $[Cd(N\text{-}POA)_2]\cdot 2H_2O$ were synthesized following the above procedure using $Co(CH_3COO)_2\cdot 4H_2O$ (0.5 mM, 0.125 g), $Ni(CH_3COO)_2\cdot 4H_2O$ (0.5 mM, 0.124 g), $Mn(CH_3COO)_2\cdot 4H_2O$ (0.5 mM, 0.123 g), $Zn(CH_3COO)_2\cdot 2H_2O$ (0.5 mM, 0.110 g), and $CdCl_2\cdot 2H_2O$ (0.5 mM, 0.110 g) instead of $Cu(CH_3COO)_2\cdot H_2O$. In the case of $[Pd(N\text{-}POA)_2]\cdot 3H_2O$, 0.5 mM (0.089 g) of $PdCl_2$ was dissolved by boiling in 5 mL concentrated HCl, cooling, and then diluting with 15 mL distilled water. To this solution was added, with stirring solution of *N*-POAH (1 mM, 0.363 g) dissolved in 50 mL chloroform/methanol mixture (1: 1, v/v). After addition was complete,

the mixture was refluxed for 30 h. The compound was then filtered, washed with diethyl ether, followed by hot methanol and dried in a vacuum desiccator.

$[Co(N\text{-}POA)_2]\cdot 3H_2O$: Orange. Yield: 0.190 g (69%); m.p.: 300°C< Anal. Calcd (%) for $C_{38}H_{30}CoN_6O_{13}$ (836.93): C, 54.49; H, 3.61; N, 10.03; Co, 7.04. Found: C, 54.05; H, 4.12; N, 10.29; Co, 6.54. Selected IR data (ν, cm^{-1}): 3332–3400 ν(NH, OH/H_2O), 1663 ν(Ph-CO), 1637 ν(C=O), 1605 ν(C=O ↔ C=N). μ_{eff}: 4.13 BM. Λ_M (10^{-3} M, in DMF, $S\,cm^2\,M^{-1}$): 2.7. UV-Vis (in DMF, nm): 244, 274, 307, 360, 404, 637, 669, 782. API-ES, m/z: 784.0 $[2L+Co]^+$ (^{60}Co isotope).

$[Ni(N\text{-}POA)_2]\cdot 2H_2O$: Light brown. Yield: 0.190 g (70%); mp: 225°C. Anal. Calcd (%) for $C_{38}H_{28}N_6NiO_{12}$ (818.7): C, 55.70; H, 3.44; N, 10.25; Ni, 7.17. Found: C, 55.82; H, 4.01; N, 10.90; Ni, 8.07. Selected IR data (ν, cm^{-1}), 3378–3440 ν(NH, OH/H_2O), 1664 ν(Ph-CO), 1645 ν(Ph-CO), 1594 ν(C=O ↔ C=N). μ_{eff}: 3.10 BM. Λ_M (10^{-3} M, in DMF, $S\,cm^2\,M^{-1}$): 4.6. UV-Vis (in DMF, nm): 236, 285, 330, 372, 407, 526, 652. API-ES, m/z: 782 $[2L+Ni]^+$ (^{58}Ni isotope).

$[Mn(N\text{-}POA)_2]\cdot 2H_2O$: Yellow. Yield: 0.235 g (87%); m.p.: 300°C< Anal. Calcd (%) for $C_{38}H_{28}MnN_6O_{12}$ (815): C, 55.96; H, 3.46; N, 10.30; Mn, 6.74. Found: C, 55.90; H, 3.71; N, 10.30; Mn, 5.98. Selected IR data (ν, cm^{-1}): 3431 (NH, OH/H_2O), 1666 ν(Ph-CO), 1638 (C=O), 1615 ν(C=O ↔ C=N). μ_{eff}: 5.62 BM. Λ_M (10^{-3} M, in DMF, $S\,cm^2\,M^{-1}$): 2.8. UV-Vis (in DMF, nm): 211, 271, 297, 363, 389, 532, 570.

$[Zn(N\text{-}POA)_2]\cdot 2H_2O$: Cream. Yield: 0.210 g (76%); m.p.: 300 °C< Anal. Calcd (%) for $C_{38}H_{28}N_6O_{12}Zn$ (822.4): C, 55.44; H, 3.40; N, 10.21; Zn, 7.95. Found: C, 55.60; H, 3.72; N, 10.60; Zn, 6.18. Selected IR data (ν, cm^{-1}): 3428 ν(OH/H_2O–NH), 1662 ν(Ph-CO), 1654 ν(C=O), 1615 ν(C=O ↔ C=N). ^{1}H-NMR (DMSO), δ 9.1 (s, NH), 8.7 (s, C–H pyrimidine), 7.0–8.3 (m, Harm), 3.5 (m, H_2O); ^{13}C-NMR (DMSO), δ 192.7, 170.1, 159.7, 155.0, 146.7, 120.8–133.6, 119.3. μ_{eff}: Dia. Λ_M (10^{-3} M, in DMF, S $cm^2\,M^{-1}$): 2.9. UV-Vis (in DMF, nm): 274, 297, 308, 329, 394.

$[Cd(N\text{-}POA)_2]\cdot 2H_2O$: Light yellow. Yield: 0.190 g (65%); m.p.: 300°C< Anal. Calcd (%) for $C_{38}H_{28}CdN_6O_{12}$ (872.4): C, 52.27; H, 3.20; N, 9.63; Cd, 12.88; Found: C, 52.56; H, 3.50; N, 9.69; Cd, 11.35. Selected IR data (ν, cm^{-1}): 3430 (OH/H_2O–NH), 1666 ν(Ph-CO), 1627 ν(C=O), 1600 ν(C=O ↔ C=N). ^{1}H-NMR (DMSO), δ 9.3 (s, NH), 8.9 (s, C–H pyrimidine), 6.8–8.3 (m, Harm), 3.5 (m, H_2O); ^{13}C-NMR (DMSO), δ 193.1, 176.5, 162.1, 157.4, 151.7, 122.5–137.6, 117.9. μ_{eff}: Dia. Λ_M (10^{-3} M, in DMF, S $cm^2\,M^{-1}$): 4.6. UV-Vis (in DMF, nm): 274, 293, 313, 364, 406.

$[Pd(N\text{-}POA)_2]\cdot 3H_2O$: Orange-brown. Yield: 0.150 g (51%); m.p.: 235°C. Anal. Calcd (%) for $C_{38}H_{30}N_6O_{13}Pd$ (884.4): C, 51.57; H, 3.42; N, 9.50. Found: C, 51.33; H, 3.46; N, 10.04. Selected IR data (ν, cm^{-1}): 3406 ν(OH/H_2O–NH), 1677 ν(-Ph-C=O), 1663 ν(C=O), 1597 ν(C=O ↔ C=N). ^{1}H-NMR (DMSO), δ 9.2 (s, NH), 8.9 (s, C–H pyrimidine), 7.2–8.7 (m, Harm), 3.4 (m, H_2O); ^{13}C-NMR (DMSO), δ 191.3, 173.1, 161.7, 153.3, 146.4, 127.8–139.6, 116.3. μ_{eff}: Dia. Λ_M (10^{-3} M, in DMF, S cm^2 M^{-1}): 18.9. UV-Vis (in DMF, nm): 205, 280, 340, 502. API-ES, m/z: 885 $[(2L+Pd)+3H_2O]^+$ (^{106}Pd isotope).

2.5. *Biological assay*

2.5.1. Compounds. Test compounds were dissolved in DMSO (12.5%) at an initial concentration 1280 $\mu g\,mL^{-1}$ and then serially diluted in culture medium.

2.5.2. Cells. Bacterial strains were supplied from American Types Culture Collection. *Candida* strains were obtained from Refik Saydam Hifzisihha Research Institute, Ankara, Turkey.

2.6. *Antibacterial assay*

The compounds were screened for their antibacterial activity against four Gram-positive (*Staphylococcus aureus* ATCC 6538, *S. aureus* ATCC 25923, *Bacillus cereus* ATCC 7064 and *Micrococcus luteus* ATCC 9345) and one Gram-negative (*Escherichia coli* ATCC 4230) bacteria as described by Clause [13] with minor modifications. Ampicillin trihydrate was used as reference antibacterial agent. The solutions of the compounds and reference drug were dissolved in DMSO at 2560 $\mu g\,mL^{-1}$. The twofold dilution of compounds and reference drug were prepared (1280, 640, 320, 160, 80, 40, 20, 10, $5 > \mu g\,mL^{-1}$). Antibacterial activities were performed in Mueller–Hinton broth (Difco) medium at pH 7.2 with an inoculum of $(1–2) \times 10^3$ cells mL^{-1} by the spectrophotometric method and an aliquot of 100 µL was added to each tube of serial dilution. The chemical compounds-broth medium serial tube dilutions inoculated with each bacterium were incubated on a rotary shaker at 37°C for 18 h at 150 rpm. The minimum inhibitory concentrations (MICs) of each compound were recorded as lowest concentration of each chemical compounds in the tubes with no growth (i.e. no turbidity) of inoculated bacteria.

2.7. *Antifungal assay*

Antifungal activities were tested against three yeast (*Candida albicans* ATCC 14053, *C. krusei* ATCC 6258 and *C. parapsilosis* ATCC 22019) strains according to the guidelines in NCCLS approved standard document M27-A using the microdilution broth procedure [14]. Fluconazole was used as reference antifungal agent. Test compounds and reference drug were dissolved in DMSO at 2560 $\mu g\,mL^{-1}$ and twofold dilution of the compounds and reference drug were prepared (1280, 640, 320, 160, 80, 40, 20, 10, $5 > \mu g\,mL^{-1}$). Antifungal activities of the yeast strains were performed in RPMI 1640 Medium (Sigma), which were buffered to pH 7.0 with 0.165 M morpholinopropanesulfonic acid (Sigma), as outlined in document M27-A. Stock yeast inoculum suspensions were adjusted to $(0.5–2.5) \times 10^3$ cells mL^{-1} by spectrophotometric method and 100 µL aliquot was added to each tube of the serial dilution. The broth medium serial tube dilutions inoculated with yeast were incubated on a rotary shaker at 37°C for 18 h at 150 rpm. MICs of each compound were recorded as lowest concentration of each chemical compounds in the tubes with no growth (i.e. no turbidity) of inoculated yeast.

3. Results and discussion

3.1. *Synthesis of the ligand and metal complexes*

The new ligand *N*-POAH, whose structure is given in figure 1, was synthesized by 1 : 1 condensation of oxalylchloride with *N*-aminopyrimidine in dry toluene. The ligand is

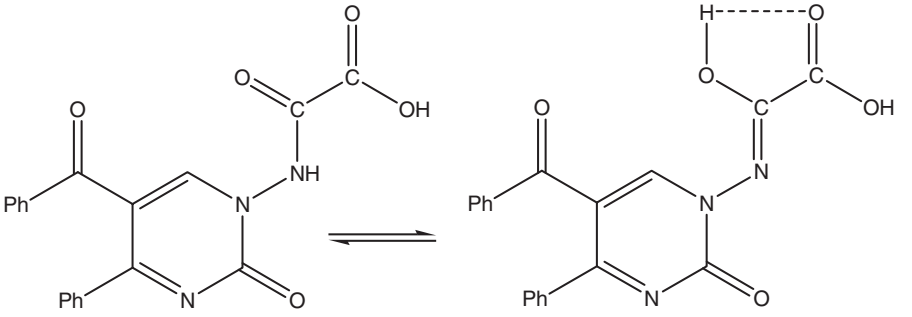

Figure 1. Structure of the ligand (*N*-POAH).

soluble in DMSO, DMF, $CHCl_3$, CH_3CN, CH_2Cl_2, and partly soluble in H_2O, MeOH, EtOH, however, insoluble in *n*-hexane and diethyl ether.

Complexes with deprotonated forms of *N*-POAH; $[Cu(N\text{-}POA)_2]\cdot 2H_2O$, $[Co(N\text{-}POA)_2]\cdot 3H_2O$, $[Mn(N\text{-}POA)_2]\cdot 2H_2O$, $[Ni(N\text{-}POA)_2]\cdot 2H_2O$, $[Zn(N\text{-}POA)_2]\cdot 2H_2O$, $[Cd(N\text{-}POA)_2]\cdot 2H_2O$, and $[Pd(N\text{-}POA)_2]\cdot 3H_2O$ were obtained from a refluxing mixture of the respective ligand and appropriate metal salts in 1 : 2 molar ratio in methanol. The complexes presented in figures 2 and 3 were formed in a reaction of equimolar amounts of an acetate/chloride salts of Cu(II), Co(II), Mn(II), Ni(II), Zn(II), Cd(II), and Pd(II) in with N-POAH in methanol solution. The complexes are soluble in dipolar aprotic solvents but sparingly soluble in common organic solvents.

3.2. *Characterization of the N-POAH and metal complexes*

3.2.1. IR spectra. *N*-POAH may exist in two tautomeric forms (figure 1) and may form intermolecular-hydrogen bonds,–N=C–O–H···O=C–OH. In IR spectra of *N*-POAH, characteristic bands appeared at 1712, ~3440, 3059, 1680, 1658, 1613 cm^{-1} corresponding to ν(COOH), ν(OH/NH), ν(C–H pyrimidine ring), ν(C=O benzoyl), ν(C=O), (–CO–NH–), respectively [15–17]. Condensation was supported by elimination of HCl from oxalylchloride and *N*-aminopyrimidine. The absence of $\nu(NH_2)$ at 3300 and 3170 cm^{-1} suggests the structure of *N*-pyrimidine oxalamic acid. The IR spectra of the complexes were compared with that of the free ligand. The disappearance of the band at 1712 cm^{-1} due to carboxylate suggests the coordination of oxygen after deprotonation. Similarly, the shifting of 1658 cm^{-1} ν(C=O) in ligand to 1627–1650 cm^{-1} in complexes indicates that keto group in the ring is also coordinating [15]. The ligand shows a broad band at 3400–3320 cm^{-1} due to asymmetric and symmetric –NH stretching frequency of –NH. The complexes show 15–60 cm^{-1} shift, indicating coordination through the amide nitrogen; the amidic νN–H (NH–C=O ↔ N=C–OH) vibration of the ligand at 1615 cm^{-1} shifts to lower frequency after complexation, between 1590 and 1600 cm^{-1}. The observed shift in C=N stretch after complexation confirms coordination of imine nitrogen to metal [10–12].

In spectra of the complexes bands at 426–465 and 488–548 cm^{-1} are due to ν(M–N) and ν(M–O), respectively [10, 11]. Broad bands of the complexes in the ~3400 cm^{-1}

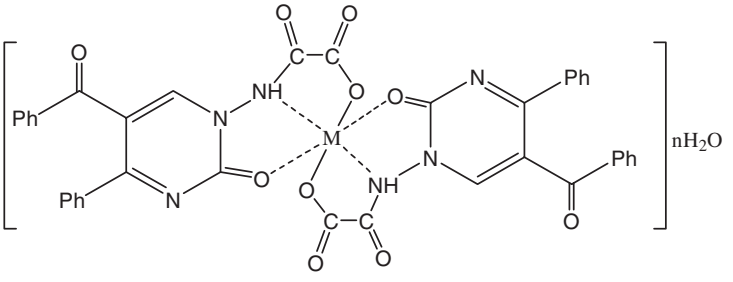

M= Cu(II), Ni(II), Mn(II), Co(II), Zn(II), and Cd(II)

Figure 2. Suggested structures of M(II) complexes of *N*-POAH.

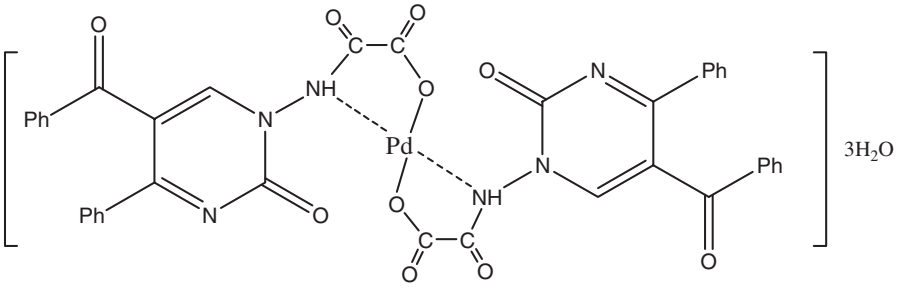

Figure 3. Suggested structure of the Pd(II) complex of *N*-POAH.

region are assigned to the ν(OH) vibration of water [17]; water content was also identified by thermal analyses.

3.2.2. UV-Vis spectral study. In the UV-Vis, the complexes show bands at approximately 325 nm and weaker bands in the range 350–410 nm. The weak bands were attributed to intramolecular charge transfer transitions from the pπ orbital on the carboxylate (phenolate) oxygen to empty d orbitals of the metal. The intense 320–330 nm bands were assigned to $\pi \rightarrow \pi^*$ (intraligand) transitions [17].

The electronic absorption spectrum of $[Cu(N\text{-POA})_2]\cdot 2H_2O$ has an absorption at 697 nm, ascribed to $^2T_{2g} \rightarrow {}^2E_g$ of the distorted octahedral environment [18]. The effective magnetic moment (μ_{eff}: 1.92 BM) is typical for distorted octahedral Cu(II) chelates.

The high spin octahedral Co(II) and Ni(II) complexes exhibit magnetic moment values of 4.2 and 3.1 BM, respectively, and three transitions each in the electronic spectra. The magnetic moment for $[Co(N\text{-POA})_2]\cdot 3H_2O$ is near the spin-only value. The electronic spectrum shows three d–d bands of weak intensity. The first band (782 nm) is assigned to the transition $^4T_{2g} \rightarrow {}^4T_{1g}(F)$, the second band (669 nm) is assigned to $^4A_{2g} \rightarrow {}^4T_{1g}(F)$, the third (637 nm), split into three components, is assigned to $^4T_{1g}(P) \rightarrow {}^4T_{1g}(F)$. The band observed at 404 nm is assigned to Co $\rightarrow$ L charge

Table 1. The MICs[a] of *N*-POAH and its metal complexes [Cd(II), Pd(II), Cu(II), Co(II), Mn(II), Zn(II)] against Gram-negative and Gram-positive bacterial strains.

Compound	*B. cereus* ATCC 7064	*S. aureus* ATCC 6538	*S. aureus* ATCC 25923	*E. coli* ATCC 4230	*M. luteus* ATCC 9345
N-POAH	640	160	160	640	160
$[Cu(N\text{-}POA)_2]\cdot 2H_2O$	40	80	40	640	160
$[Co(N\text{-}POA)_2]\cdot 3H_2O$	160	80	160	160	160
$[Mn(N\text{-}POA)_2]\cdot 2H_2O$	640	640	640	640	640
$[Ni(N\text{-}POA)_2]\cdot 2H_2O$	160	160	160	320	160
$[Zn(N\text{-}POA)_2]\cdot 2H_2O$	640	320	320	640	320
$[Cd(N\text{-}POA)_2]\cdot 2H_2O$	320	640	640	640	320
$[Pd(N\text{-}POA)_2]\cdot 3H_2O$	320	320	320	640	320
Ampicillin	5	5	10	20	10

[a]The MICs values were determined as $\mu g\,mL^{-1}$ active compounds in medium.

transfer [18]. $[Ni(N\text{-}POA)_2]\cdot 2H_2O$ exhibits three spectral bands at 407, 526, and 652 nm. The first is due to charge transfer, the last two bands are assigned to octahedral spin allowed $^3A_{2g} \rightarrow {}^3T_{1g}(F)$ and $^3A_{2g} \rightarrow {}^3T_{2g}(F)$ transitions. The room temperature μ_{eff} 3.1 BM and the spectral data support octahedral geometry [19].

$[Mn(N\text{-}POA)_2]\cdot 2H_2O$ gave three peaks at 363, 389, and 532 nm and room temperature μ_{eff} 5.62 BM. The first two bands are due to the effect of metal on the π–π^* electronic transition of the free ligand. However, the band at 532 nm is identified to d–d electronic transition for high-spin octahedral configuration.

The d^8 square planar $[Pd(N\text{-}POA)_2]\cdot 3H_2O$ complex is expected to exhibit three spin-allowed d–d transitions corresponding to $^1A_{1g} \rightarrow {}^1A_{2g}$, $^1A_{1g} \rightarrow {}^1B_{1g}$ and $^1A_{1g} \rightarrow {}^1E_g$, respectively. However, the strong CT band, L→M at *ca* 380 nm in this complex, tails into the visible region, obscuring d–d bands [20].

3.2.3. NMR spectral study. DMSO-d_6 was used as a solvent to measure the ^{1}H-, ^{13}C-NMR spectra of the *N*-POAH and its Zn(II), Cd(II) and Pd(II) complexes. Slightly broad and medium resonances at δ 12.4 and 9.1 ppm are due to COOH proton and NH of the ligand. The singlet at δ 8.7 ppm is due to pyrimidine ring (C(6)-H) proton. In the spectra of *N*-POAH, the phenyl multiplet was at δ 6.8–7.9 ppm. ^{13}C-NMR spectra of the ligand have a cluster of peaks at δ 191.3, 173.7, 153.9, 151.7, 116.8 ppm due to benzoyl carbon, carbon of the carboxyl group, C(2)-, C(6)-, C(5)-pyrimidine ring, respectively. The spectrum of the ligand show peaks at δ 118.55–136.91 ppm due to phenyl carbons and one at δ 157.7 ppm, which may be attributed to –CO–NH–.

The complexes were also investigated by ^{1}H-and ^{13}C-NMR in DMSO-d_6 where the data (given in section 2) are in agreement with coordination through the carboxylate (disappearance of the H(1) signal in) and the peaks characteristic for water molecules were observed around δ 3.52 ppm.

3.3. *Mass spectra*

In the mass spectra of the ligand and its metal complexes, peaks are attributable to the molecular ions; *m/z*: 362 $[L]^+$, *m/z*: 701 $[(2L+Cu)-2CO_2]^+$, *m/z*: 784 $[2L+Co]^+$, *m/z*:

782 $[2L+Ni]^+$, *m/z*: 885 $[(2L+Pd)+3H_2O]^+$. The spectrum of the Pd(II) complex is shown in "Supplementary material".

3.4. *Thermal decomposition*

The thermal behavior was studied using TGA and DTA techniques under nitrogen at 30–1100°C. The complexes decompose in two or three steps into MO as final product from which the metal content can be calculated *via* AAS technique and compared with that obtained from the elemental analysis. For all complexes, the analytical data show a weight loss, which occurs in the temperature range 42–103°C, corresponding to loss of crystal water. This weight loss is 4.2% in the case of Cu(II) complex, in agreement with the empirical formula $[Cu(N\text{-POA})_2]\cdot 2H_2O$ (theoretical weight loss 4.4%). For the $[Ni(N\text{-POA})_2]\cdot 2H_2O$ complex, the weight loss is equal to 4.6% (theoretical weight loss 4.4%) and is equal to 6.7% for the $[Co(N\text{-POA})_2]\cdot 3H_2O$ complex (theoretical weight loss 6.5%).

For Cu(II) complex, the initial weight loss at 43–101°C, with corresponding endothermic peak at 67°C, is interpreted as loss of coordinated water. The second step of decomposition corresponds to the loss of ligand from the anhydrous complex at 101–850°C with an exothermic peak at 313°C. The third step of decomposition occurred at 850–1000°C, associated with exothermic peak at 924°C leading to CuO and C.

3.5. *Electrochemical studies*

Redox properties of *N*-POAH and its metal complexes were investigated at glassy carbon electrode in DMSO (except for Pd(II) complex, which was studied in DMF) containing $0.1\,M\,L^{-1}$ $LiClO_4$ by cyclic voltammetry.

In the potential range of $-2.3+1.2\,V$ at scan rate of $100\,mV\,s^{-1}$, the cyclic voltammogram of *N*-POAH has four cathodic waves (Ic, IIc, IIIc, and IVc) with their anodic partners (Ia, IIa, IIIa, and IVa) (Supplementary material). The difference between cathodic and anodic peak potentials reveals that the electrode reaction is not reversible. Such irreversibility is observed at the entire scan rates of investigation ($10–500\,mV\,s^{-1}$). At scan rate above $50\,mV\,s^{-1}$, Ia, and IIa were fused into only one broad peak. The cathodic wave IIc was also in the form of a peak and was easily measurable. Hence, all subsequent work is based on measurement of the magnitude of this step. A plot of logarithm of peak current *versus* logarithm of scan rate gave a straight-line (correlation coefficient 0.999) with a slope of 0.52, very close to the theoretical value of 0.5, which is expected for an ideal reaction of solution species [21], so in this case the process had a diffusive component. A slightly negative shift in the peak potential was observed, which confirms the irreversibility of the process, with the simultaneous increase in the peak current when the scan rate was increased. With the reported data concerning electrochemical behavior of 1-amino-5-benzoyl-4 phenyl-1H-pyrimidine-2-one, at a hanging mercury drop electrode in aqueous and non-aqueous methanol, we assume that reductions of *N*-POAH are located on the secondary amino and the carbonyl of pyrimidine ring at positions 1 and 2, respectively.

On the cathodic side, the cyclic voltammogram of Cu(II) complex (Supplementary material) shows four cathodic peaks (I′c, II′c, III′c, and IV′c) in addition to the ligand peaks. On the reverse scan, oxidation waves Ia, Iia, and IIIa are absent; however, there

is a new oxidation step (IV′a) at more positive potential. Wave IV′c, which was near the cathodic window of the $LiClO_4$/DMSO system, only appeared when waves I′c, II′c and III′c were present on the initial scan. By scanning to less negative potentials than wave IV′c, the absence of oxidation wave IV′a on the reverse scan indicates that IV′a is due to a product formed at potential of wave IV′c. The reduction wave of IV′c may be attributable to $[[Cu^{I}L_2]]/[Cu^{0}L_2]$, with associated response (oxidation wave IV′a) in the reverse scan. However, when the scan was limited to less negative potentials than the potential of wave IV′c, one sharp and well-defined oxidation peak (I′a) with a shoulder (II′a) and a small one (III′a) (at more positive potential) were produced. If successive cyclic scans are made, the main oxidation peak increased as the number of scans increased. We should bear in mind that [22, 23] after one-electron reduction corresponding to $[[Cu^{II}L_2]]/[[Cu^{I}L_2]]$, part of $[[Cu^{I}L_2]]$ decomposes into copper metal (reaction 1). Therefore, it may be assumed that the corresponding anodic waves (I′a–III′a) are associated with the reoxidation of electrodeposited copper metal to free Cu^{+} and Cu^{2+} according to reaction 2 shown as follows:

$$[Cu^{I}L_2] \leftrightarrow Cu^{+}\ 2L + e^{-} \leftrightarrow Cu^{0} + 2L \tag{1}$$

$$Cu^{0} - e^{-} \leftrightarrow Cu^{+} - e^{-} \leftrightarrow Cu^{2+} \tag{2}$$

In the cyclic voltammogram of the complex with Co(II), in addition to ligand waves Ic (−1.14 V) and IIc (−1.55 V), there is an ill-defined reduction wave III′c (−1.59 V) and one broad oxidation peak at +0.62 V. The cathodic wave III′c (−1.59 V) corresponds to the reduction of complexed Co^{II} to Co^{0}. Finally, Co^{0} is oxidized to coordinated Co^{II} because this peak disappears when the sweep is limited to less negative potentials than the potential of wave III′c (−1.59 V). After the first voltammetric cycle, the current intensities of the waves decreased rapidly, which may be explained by a rapid decomposition reaction, yielding a solid product that deposit at the electrode surface.

For the Mn(II) complex, when the potential was first scanned in the negative direction, in addition to ligand waves Ic (−1.43 V) and IIc (−1.53 V), one irreversible reduction wave III′c (−2.13 V) was observed with a corresponding anodic wave III′a (−0.40 V). Reversing the scan before reduction wave III′c shows the absence of III′a (−0.40 V). When the scan was initiated in the positive direction, two-step oxidation processes (I′′a (+0.51 V) and II′a (+0.72 V)) with corresponding cathodic waves (I′c (+0.40 V) and II′c (+0.59 V)) were observed. Since the difference of anodic and cathodic potentials was about 100 mV, this process was quasi-reversible. Reductive and oxidative processes (III′c/III′a and I′a, II′a/I′c, II′c) are based on the manganese center.

The electrochemical behavior of nickel(II) complex is similar to that of *N*-POAH, with anodic waves shifted to lower positive potential. This suggests that the oxidation of the Ni(II) complex is a ligand-based process. In the case of complexes with Zn(II) and Cd(II), very poorly defined anodic waves were observed.

The cyclic voltammograms of Pd(II) complex were recorded in DMF containing 0.1 M L^{-1} $LiClO_4$. *N*-POAH in DMF from −2.3 to +1.5 V shows three cathodic (−1.40, −1.540, and −1.82 V) and two anodic (+0.26 and + 0.987 V) waves. On the cathodic side, the Pd(II) complex shows two new waves (−0.75 and −2.10 V), which can be attributed to Pd^{II}/Pd^{I} and Pd^{I}/Pd^{0} reduction.

The electrochemical data upon the electrode potentials are reported in table 2.

Table 2. Voltammetric results in *V vs.* Ag/AgCl.

Compound	*E*c	*E*a
N-POAH	Ic:−1.23, IIc:−1.55, IIIc:−1.89, IVc:−2.05	Ia+IIa:+0.04, IIIa:+0.52, IVa:+1.00
$[Cu(N\text{-}POA)_2]\cdot 2H_2O$	I′c:+0.11, II′c:−0.26, III′c:−0.57, Ic:−1.35, IIc:−1.55, IIIc:−1.85, IVc:−2.03, IV′c:−2.20	I′a:+0.05, II′a:+0.22, III′a:+0.42, IVa:+0.82, IV′a: +1.2
$[Co(N\text{-}POA)_2]\cdot 3H_2O$	Ic:−1.14, IIc:−1.55, III′c:−1.95	I′a:+0.62
$[Mn(N\text{-}POA)_2]\cdot 2H_2O$	II′c:+0.59, I′c:+0.40, Ic:−1.43, IIc:−1.53, III′c:−2.13	III′a:−0.40 I′a:+0.51, II′a:+0.72
$[Ni(N\text{-}POA)_2]\cdot 2H_2O$	Ic:−1.31, IIc:−1.54, IIIc:−1.92, IVc:−2.10	Ia+IIa:−0.20, IIIa:+0.29, IVa:+0.68
$[Zn(N\text{-}POA)_2]\cdot 2H_2O$	Ic:−1.42, IIc:−1.55, IIIc+IVc:−2.05	
$[Cd(N\text{-}POA)_2]\cdot 2H_2O$	Ic:−1.40, IIc:−1.52, IIIc:−1.88, IVc:−2.07	
$[Pd(N\text{-}POA)_2]\cdot 3H_2O$	I′c:−0.75, Ic:−1.40, IIc:−1540, IIIc:−1.82, IV′c:−2.10	I′a:+0.26, II′a:+0.61

ν denotes 100 mV s^{-1}; *E*c, cathodic; and *E*a, anodic.

A plot of logarithm of peak current significantly correlates with the logarithm of scan rate for Cu(II), Ni(II), and Pd(II) complexes with slopes of 0.47 (correlation coefficient 0.997), 0.44 (correlation coefficient 0.996), and 0.51 (correlation coefficient 0.965), respectively, showing that redox processes are predominantly diffusion-controlled in the whole scan rate range studied. Due to poorly resolved signal obtained by cyclic voltammetry, the effect of potential scan rate on Co(II), Mn(II), Cd(II), and Zn(II) complexes was not evaluated.

3.6. *Biological results*

Antimicrobial activities of the newly synthesized compounds were screened against four Gram-positive (*S. aureus* ATCC 6538, *S. aureus* ATCC 25923, *B. cereus* ATCC 7064 and *M. luteus* ATCC 9345), one Gram-negative (*E. coli* ATCC 4230) bacteria and three yeast (*C. albicans* ATCC 14053, *C. krusei* ATCC 6258 and *C. parapsilosis* ATCC 22019) strains by using broth microdilution. Ampicillin trihydrate for bacteria and fluconazole for yeast were used as reference drugs. MICs against bacterial and fungal strains are shown in table 1. The ligand and complexes exhibit weak activity against the tested microorganisms with MICs in the range of 160–640 μg mL^{-1}, except for the Cu(II) complex. The Cu(II) complex displayed selective and effective antibacterial activity against one Gram-positive spore-forming bacterium (*B. cereus* ATCC 7064), two Gram-positive bacteria (*S. aureus* ATCC 6538, *S. aureus* ATCC 25923) at 40–80 μg mL^{-1}, and poor activity against other bacterial strains (*E. coli* ATCC 4230, *M. luteus* ATCC 9345). The Co(II) complex was moderate inhibitor against one Gram-positive bacterium as *S. aureus* ATCC 25923 (MIC value 80 μg mL^{-1}). The Cu(II) complex had more antibacterial activity than uncomplexed ligand and other complexes. The activity of complexes was enhanced by coordination. The data are in agreement with the previous studies that Cu(II) complexes of the various compounds have greater activity toward microorganisms than the free ligands [24–26]. Generally, chelation/coordination of the metal results in higher capability to penetrate microorganisms through the lipopolysaccharide layer of the cell membrane [27, 28].

Only the Cu(II) complex exhibited weak antifungal activity (MICs, 640 $\mu g\,mL^{-1}$) against *C. albicans* ATCC 14053, *C. krusei* ATCC 6258 and *C. parapsilosis* ATCC 22019.

4. Conclusion

Synthesis, spectroscopic characterization, electrochemical study, and antimicrobial investigation of a substituted pyrimidine ligand and its mononuclear complexes have been presented. We evaluated *in vitro* antibacterial and antifungal activities of new synthesized various metal complexes of *N*-POAH which had weak antimicrobial effects against tested microorganisms, except $[Cu(N\text{-}POA)_2]\cdot 2H_2O$ which had good antibacterial activity. The reason for higher antibacterial activity can be ascribed to the effect of copper on vital cell process, such as deactivating several structural enzymes which play important roles in metabolic pathways of the microorganisms.

Acknowledgment

We are grateful to Scientific and Research Council of Turkey (TBAG 105T145) for the support of this research.

References

[1] A. Darwanto, L. Ngo, L.C. Sowers. *Adv. Mol. Toxicol.*, **2**, 153 (2008).
[2] R. Hilal, Z.M. Zaky, S.A.K. Elroby. *Spectrochim. Acta A*, **63**, 740 (2006).
[3] S.I. Mostafa, M.A. Kabil, E.M. Saad, A.A. El-Asmy. *J. Coord. Chem.*, **59**, 279 (2006).
[4] F.A. French, E.J. Blanz Jr, D.A. French. *J. Med. Chem.*, **13**, 1117 (1970).
[5] J.H. Cory, A.E. Fleischeher. *Cancer Res.*, **39**, 4600 (1979).
[6] T. Hitoshi, N. Tamao, A. Hideykki, F. Manalou, M. Takayuki. *Polyhedron*, **16**, 3787 (1997).
[7] P. Arranz-Mascarós, M.D. Gutiérrez-Valero, R. López-Garzón, M.D. López-León, M.L. Godino-Salido, A. Santiago-Medina, H. Stoeckli-Evans. *Polyhedron*, **27**, 623 (2008).
[8] M.T. Madigan, J.M. Martinko, J. Parker. *Brock Biology of Microorganisms*, 8th Edn, Prentice-Hall, Inc., Upper Saddle River, New Jersey, USA (1997).
[9] M.A. Girasolo, C. Di Salvo, D. Schillaci, G. Barone, A. Silvestri, G.J. Ruisi. *Organomet. Chem.*, **690**, 4773 (2005).
[10] M. Sönmez, İ. Berber, E. Akbaş. *Eur. J. Med. Chem.*, **41**, 101 (2006).
[11] N.R. Mohamed, M.M.T. El-Saidi, Y.M. Ali, M.H. Elnagdi. *Bioorg. Med. Chem.*, **15**, 6227 (2007).
[12] Y. Akçamur, B. Altural, E. Sarıpınar, G. Kollenz, O. Kappe, K. Peters, E. Peters, H. Schering. *J. Heterocylic Chem.*, **25**, 1419 (1988).
[13] G.W. Clause. *Understanding Microbes: A Laboratory Textbook for Microbiology*, W.H. Freeman and Company, New York, USA (1989).
[14] A. Villanova. *National Committee for Clinical Laboratory Standards*, **17**, 1 (1997).
[15] H.L. Hu, C.W. Yeh, J.D. Chen. *Eur. J. Inorg. Chem.*, 4696 (2004).
[16] K. Nakamoto. *Infrared and Raman Spectra of Inorganic and Coordination Compounds*, Wiley, New York (1986).
[17] G. Asgedom, A. Streedhara, J. Kivikoski, E. Kolehmainen, C.P. Rao. *J. Chem. Soc., Dalton Trans.*, 93 (1996).
[18] A.B.P. Lever. *Inorganic Electronic Spectroscopy*, Elsevier, Amsterdam (1984).
[19] B.N. Figgis, J. Lewis. *Progress in Inorganic Chemistry*, Vol. 6, Wiley Interscience, New York (1964).
[20] S.S. Kandil, S.M.A. Katip, N.H.M. Yarkandi. *Transition Met. Chem.*, **32**, 791 (2007).

[21] E. Laviron. *J. Electroanal. Chem.*, **112**, 11 (1980).
[22] P. Zanello. *Inorganic Electrochemistry; Theory, Practice and Application*, The Royal Society of Chemistry, Cambridge (2003).
[23] M. Aguilar-Martinez, R. Saloma-Aguilar, N. Macias-Ruvalcaba, R. Cetina-Rosado, A. Navarrete-Vazquez, V. Gomez-Vidales, A. Zantella-Dehesa, R.A. Toscano, S. Hernandez-Ortega, J.M. Fernandez-G. *J. Chem. Soc., Dalton Trans.*, 2346 (2001).
[24] X.Y. Xu, J. Gao, M.Y. Wang, W.X. Ma, H.B. Song, K.P. Wainwright. *J. Coord. Chem.*, **58**, 669 (2005).
[25] A.A. Massoud, V. Langer, L. Öhrstrom, M.A.M. Abu-Youssef. *J. Coord. Chem.*, **62**, 519 (2009).
[26] K.V. Sharma, V. Sharma, R.K. Dubey, U.N. Tripathi. *J. Coord. Chem.*, **62**, 493 (2009).
[27] Z.H. Chohan, H. Pervez, A. Rauf, C.T. Supuran. *Met. Based Drugs*, **8**, 42 (2002).
[28] Z.H. Chohan, C.T. Supuran, A. Scozzafava. *J. Enzyme Inhib. Med. Chem.*, **18**, 1 (2003).